Some Capabilities of a Joint GPS-LEO Navigation System

M. Rabinowitz, B.W. Parksinson, J.J. Spilker

September 20, 2000

Abstract

The last year has seen increasing commercial interest in the combined use of positioning and two-way communication, in applications ranging from emergency roadside assistance to location-based merchandising. These systems typically involve low-cost co-located GPS receivers and communication transceivers, where the latter device is used solely for voice or data transfer. LEO satellite systems, such as Orbcomm and Globalsltar, provide wide coverage for their data and/or voice services. We describe how the combined use of GPS and LEO signals can considerably enhance navigation performance, and ameliorate other shortcomings of GPS. The geometric diversity achieved by the telecom satellites enables the rapid, robust resolution of integer cycle ambiguities. We discuss the data reduction algorithm that has been implemented to rapidly resolve centimeter-level position without the use of ground-based pseudolites, or dual-frequency GPS receivers. In addition, using Orbcomm satellites, we experimentally demonstrate the system performance in terms of accuracy, and integrity of navigation solutions. We describe the considerable advantages provided by LEO satellites in lossy environments, or multipath-prone environments. Techniques are described which use LEOs to satisfy the FCC's E911 performance requirements when GPS signals are not trackable, such as indoors.

1 Overview of Current and Future LEO Constellations

The Global Positioning System was designed to achieve positioning accuracy, outdoors, on the order of 10 meters. Until a third civil signal [6, 7] becomes active, GPS cannot facilitate rapid robust acquisition of centimeter-level position. In addition, GPS does not operate in most indoor environments, is not reliable in urban canyons and, of course, does not offer two-way communication capability. Some burgeoning markets are substantially hindered by these shortcomings. This paper addresses how LEO augmentation of GPS can address these needs.

The table 1 summarizes pertinent technical information for some of the primary LEO constellations under construction, or in orbit [1]. Additional high bandwidth LEO fleets, mostly operating in Ku-band, are planned for launch in the next few years but will not be explicitly discussed here.

FAISAT, operated by Final Analysis Inc., is geared towards the wireless messaging and remote internet access markets. They have established partnerships with Raytheon, General Dynamics and L-3 Communications, and are planning to begin operation in 2002.

[1] We only present information that is available in the public domain. This information is not necessarily up-to-date.

	Globalstar	Iridium	Orbcomm	ECCO	FAISAT	LEO One
Altitude(km)	1400	780	820	2035	1000	950
Position sensing	GPS	tracking	GPS	unknown	GPS	GPS
Operational Satellites	48	66	35	45	32	48
User downlink band	S band	L band	VHF,UHF	S band	VHF,UHF	VHF,UHF
Average no. visible (CONUS)	2	1	1	2	1	1
Multiple access method	CDMA	TDMA FDMA	TDMA FDMA	CDMA	TDMA	FDMA
Inclination (deg)	52	86.4	45,70,108	0, 62	83, 51	50

Table 1: Six of the Big LEO Constellations

LEO One, operated by dBX Corporation, is pursuing the market of near real-time short messaging. They have established partnerships with DaimlerChrysler and Lockheed Martin, and expect to be operational by 2003. ECCO is designed for satellite telephony and is operated by Constellation Communications, with substantial investment from Orbital Sciences Corporation. The company plans to have 10 operational satellites in equatorial orbit which will begin operation in 2002. These will purportedly be joined by an additional 35 satellites for Global Coverage at a later date. Orbcomm, operated by Orbital Sciences Corporation and Teleglobe, is geared towards the low data rate messaging market. Their satellites have been in continuous operation since 1998. Iridium, which was pursuing the global mobile telephony market, began operation in 1999, but filed Chapter 11 and ended commercial service in August 2000. However, in October 2000, Boeing has emerged as a potential new operator of the Iridium Satellites. Globalstar is geared towards the global portable telephony and data markets. They began service in 2000.

2 System Concept

An overview of the joint GPS/LEO system [10, 11, 5, 9, 8] is presented in fig.1. The user and reference receivers track the incident phase of the LEO and GPS signals. In addition, the reference receives up-to-date ephemeris information from the relevant satellites [2]. The reference information is conveyed to a control center where the differential corrections, and other navigational aids, are computed. This differential data is conveyed to the user receiver [3] via a satellite data channel, or via terrestrial infrastructure. Thus far, only a terrestrial data connection has been employed. By using reference code or carrier prediction techniques, the data channel need be

[2] Both Orbcomm and Globalstar have onboard GPS receivers

[3] Or to the point, such as a cellular base-station, where user position is computed

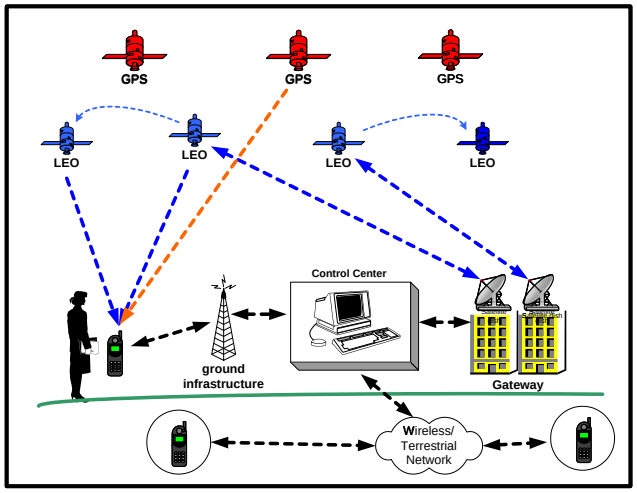

Figure 1: Architectural Overview of the LEO Concept

active in bursts, at most every 5 seconds, where each burst conveys under 1 Kbit of data.

For precision navigation, the receivers track the absolute carrier phase of the LEO and GPS signal. The geometric diversity achieved primarily by the motion of the LEOS enables the user receiver to resolve the integer cycle ambiguities on the Navstar satellite signals as well as parameters related to the cycle ambiguities on the LEO signals, and consequently to position itself with centimeter-level accuracy in the absence of multipath. In most applications, however, centimeter-level accuracy is redundant, and multipath dominates the noise equation. If the LEO is transmitting a CDMA signal, as in the case of Globalstar, that signal can be used to position the user, even when GPS is not available, such as for lossy indoor environments. Ideally, a receiver would track at least 2 LEO satellites, 100% of the time. We will focus our attention on the Orbcomm and Globalstar, which are the only constellations currently in operation. Fig.2 (left) indicates the fraction of time that 1,2,3 and 4 Globalstar satellites are visible above 10^o mask angle for various latitudes [4]. Fig.2

[4] This plot ignores the fact that a satellite may sometimes not

(right) addresses the combined Orbcomm and Globalstar fleets. Although there are 35 Orbcomm satellites in orbit, the arrangement of this constellation is currently suboptimal for coverage of the CONUS. Nonetheless, these additional signals would substantially enhance robustness to signal blockages, cycle slips, as well as system GDOP. In addition, the enhanced availability of RAIM [14] geometries is considerable [10, 8].

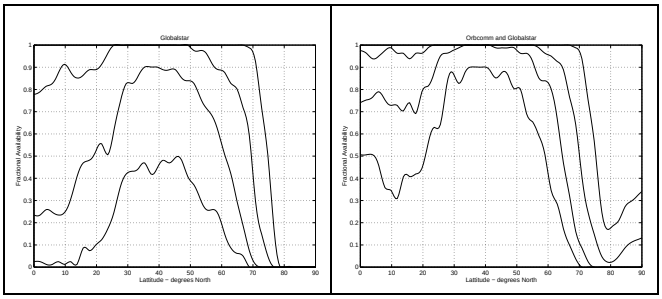

Figure 2: Availability study, using Keplerian Two-Line-Elements, for the Globalstar Satellites (left) and for Orbcomm/Globalstar combined.

3 The Use of LEOS in Disadvantaged Environments

3.1 Characterizing the Problem

Fig.'s 3 and 4 [19, 17, 16], taken from NASA/JPL studies, characterize the indoor effects on L-band (GPS) and S-band (Globalstar) signals. The attenuation on signals within each building is measured relative to the signal power outside, with a direct line of site to the signal source. Fig. 4 illustrates the dependence of attenuation on frequency. This data was taken in a farmhouse, which displayed the strongest negative trend, shown as a solid line. In general - as shown by fig. 3 - there is no clear trend, however there is considerable fine structure with respect to frequency [5], due to interference from multipath indoors. From fig 3, we see that 95% of the S-band signal energy shows less than 30dB of attenuation, in most buildings. Hence, we adopt 30dB of attenuation as our performance objective.

Fig. 5 describes the fraction of signal energy for which the delay caused by multipath is less than a certain time. Data was taken in a room, a metal shack and the foyer of a large building [18]. For example,

be illuminated by a Gateway. This effect depends strongly on longitude and will have a slight impact on signal availability.

[5] This fine structure will translate to considerable power variations as the antenna is shifted spatially

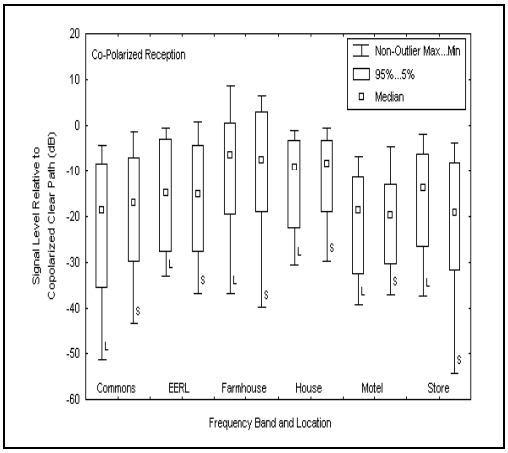

Figure 3: Attenuation of L-band and S-band signals in a range of indoor settings

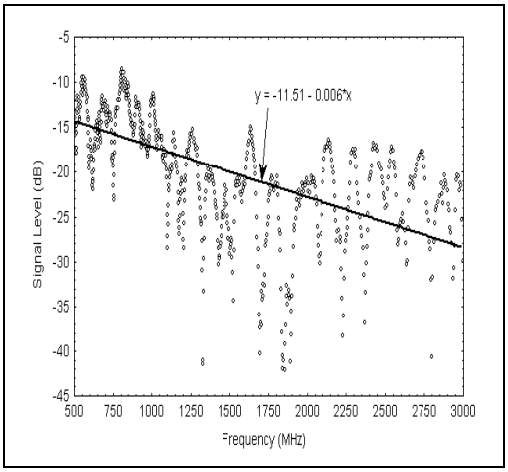

Figure 4: Dependence of attenuation on frequency in a farmhouse

consider the foyer of the large building. The graph indicates that roughly 95% of the signal energy is delayed by less than 100ns.

3.2 Integrating Attenuated Signals

The SNR of an incident signal is enhanced in inverse proportion to the bandwidth of the DLL filter, or similarly, the post-correlation integration time. There are four fundamental limitations, however, on how long a satellite signal may be integrated:

- *Data.* All techniques for integrating a signal longer than one data symbol period bear a substantial noise penalty. In the case of GPS, which has a 50Hz data rate, the best solution is to feed-forward

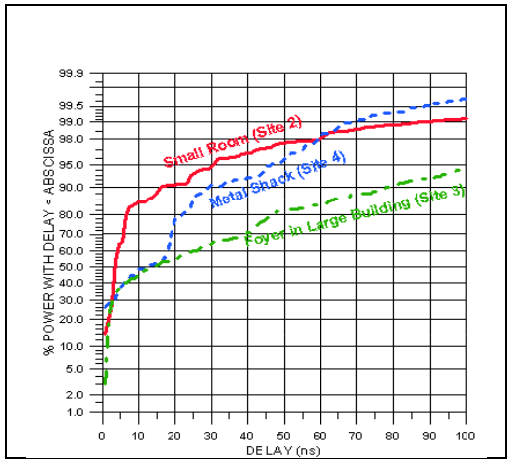

Figure 5: Cumulative Distribution Function of Signal Energy vs Delay

the GPS data by some other real-time data channel so that a receiver may post-correct the GPS data bit flips. This can be achieved, for example, by installing a network of servers at cellular base stations to transmit the additional information [12]. In the case of LEOS this problem can be entirely circumvented, since there are signals which are either of known modulation, or are unmodulated.

- *Oscillator Stability.* Whatever the receiver implementation, the PLL control cannot be updated for the duration that a signal is being integrated. Hence, it is necessary that the local oscillator not drift out of phase by more than π during the integration period. This short-term stability of an oscillator is governed by Allan Variance [4]. A quartz oscillator has an Allan Variance of better than 10^{-10} over periods of 1 second [4], which would accommodate an integration period of roughly 200 msec at S-band.

- *Ephemeris.*A receiver must predict carrier Doppler rate in order to maintain lock on a severely attenuated satellite signal. Although a tracking loop may employ a carrier-refinement algorithm [9] to identity a Doppler *offset*, the Doppler *rate* estimate cannot be updated over the period of integration. If we don't know exactly where the satellite is, we cannot correctly accommodate the change in Doppler over the course of the integration. For the Globalstar satellite altitudes, the ephemeris should be know to within 10 km for 200 msec of integration.

- *Platform Dynamics.* Of course, if the platform is accelerating, this will effect the incident signal phase. The acceleration should be less than $\frac{\lambda}{T^2}$ where T is the integration time, or roughly 3m/sec^2 for S-band at 200msec integration time.

3.3 Multipath Mitigation using Bandwidth

We perform a conservative analysis to calibrate the effects of multipath on navigation error, given the bandwidth of a signal. We begin by considering the effects of multipath for the C/A code GPS signal. Based on the data of fig.5, a conservative model assumes the multipath signal has 10dB less power than the direct signal, and is delayed by 100nsec. The effect of this signal is illustrated in fig. 6.

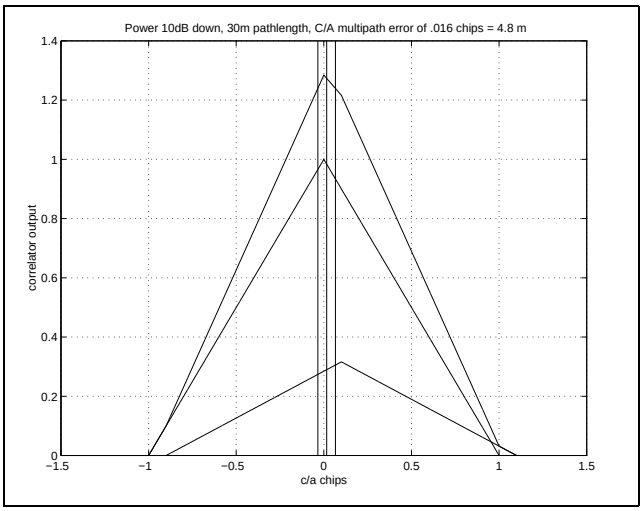

Figure 6: Effect of multipath on C/A code correlator, for infinite pre-correlation bandwidth, multipath power down 10dB and delay of 100nsec

The figure describes the output of a correlator which combines the incident GPS C/A code with a locally generated spreading sequence. The pre-correlation bandwidth is assumed to be infinite. The correlator output for a signal without multi-path is symmetrical around 0. The correlator output for the multipath signal is also shown. When the correlator locks onto the combined signal, using an early-late correlator spacing of .1 chips [15, 3] the induced error is .016 chips, or 4.8 meters. Now, consider a wide bandwidth signal of the form

$$\begin{aligned} y(t) = & D_{i1}(t)C_{i1}(t)cos\left((\omega+\omega_0)t+\phi_0(t)\right) \\ & +D_{q1}(t)C_{q1}(t)sin\left((\omega+\omega_0)t+\phi_0(t)\right) \\ & +D_{i2}(t)C_{i2}(t)cos\left((\omega-\omega_0)t+\phi_0(t)\right) \\ & +D_{q2}(t)C_{q2}(t)sin\left((\omega-\omega_0)t+\phi_0(t)\right) \end{aligned} \quad (1)$$

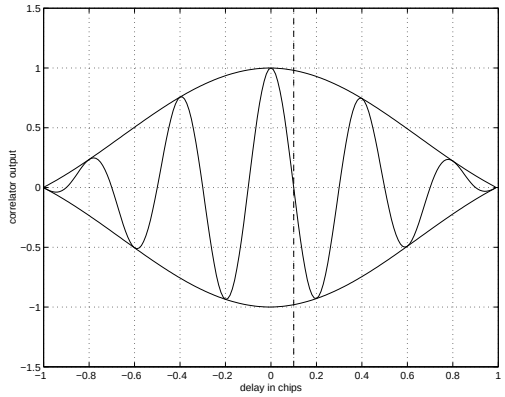

Figure 7: Autocorrelation function for the baseband signal derived from y(t), assuming that $\omega_0 = \frac{2.5}{T}$.

This signal is similar to the proposed *Split Spectrum* for modernizing GPS [6, 7, 2], but it is generalized in that different spreading codes are used for both I and Q, as well as upper and lower sidebands. We assume that upper and lower sidebands arrive at the receiver with similar phase shifts, $\phi_0(t)$. This will restrict ω_0 so as to limit differential ionospheric delay on the upper and lower sidebands. Assume that all codes have a chipping rate, T, a normalized auto-correlation function, $R(\tau)$, and that the cross-correlation energy for different codes is negligible. We may convert to a baseband signal by mixing with $2cos\left(\omega(t) + \phi_0(t)\right)$ and lowpass filtering. If T_i, the integration time of the correlator, is an integer multiple of $\frac{2\pi}{\omega_0}$, the autocorrelation function for the baseband signal simplifies to $R_y(\tau) = R(\tau)cos(\omega_0\tau)$. An example of such an autocorrelation function is illustrated in fig. 7 where we assume that the codes $C(t)$ have been filtered to a one-sided bandwidth of $1/T$Hz and that $\omega_0 = \frac{5\pi}{T}$.

As before, we model multipath as a signal, $m(t)$, with a delay of $\delta = 100ns$. Assuming $\frac{1}{T} = 1$MHz, the correlation for this delayed signal would be symmetrical around the vertical line at .1 chips, indicated in fig. 7. The combined correlation function for the direct signal, $y(t)$, and multipath signal, $m(t)$, would then be $R_y(\tau) + \alpha R_y(\tau - \delta)$ where $\alpha = \frac{max_t\ m(t)}{max_t\ y(t)}$. Notice we have assumed that $m(t)$ is perfectly in phase with $y(t)$. This is conservative since an out-of-phase $m(t)$ would in general cause less distortion of the correlation function. To find the multipath-induced error, assume equality of the early and late correlator outputs:

$$0 = R_y(\tau + \frac{d}{2}) + \alpha R_y(\tau + \frac{d}{2} - \delta) \\ -R_y(\tau - \frac{d}{2}) - \alpha R_y(\tau - \frac{d}{2} - \delta) \quad (2)$$

Perform a first-order expansion of this equality with respect to τ, and solve for τ, using the fact that R_y is symmetrical around 0, to obtain the pseudorange error due to $m(t)$:

$$\tau_e = \frac{\alpha R_y\left(-\frac{d}{2} - \delta\right) - \alpha R_y\left(\frac{d}{2} - \delta\right)}{R'_y\left(\frac{d}{2}\right) - R'_y\left(\frac{d}{2}\right) + \alpha R'_y\left(\frac{d}{2} - \delta\right) - \alpha R'_y\left(-\frac{d}{2} - \delta\right)} \quad (3)$$

If $m(t)$ is substantially delayed, the curvature of R_y at $-\delta$, $R''(-\delta)$ will be negligible. So, for $d << 1$, we can approximate $R'\left(\frac{d}{2} - \delta\right) = R'\left(-\frac{d}{2} - \delta\right)$. [6] For $d << 1$, we may expand equ.(3) to first order in d, to find

$$\tau_e = \frac{-\alpha R'_y(-\delta)}{R''_y(0)} \quad (4)$$

As expected, the numerator is proportional to the magnitude of $m(t)$, and the slope of R at the delayed time δ. From Fourier Analysis [13], it is straightforward to show that the denominator is related to the square of the signal's *Gabor Bandwidth*:

$$R''(0) = \frac{\int_\infty^\infty S_y(f) f^2 df}{\int_\infty^\infty S_y(f) df} \quad (5)$$

where S_y is the power spectral density of $y(t)$, and the denominator arises since R_y is normalized such that $R_y(0) = 1$. Clearly, the worst-case multipath effect is minimized by a signal with larger Gabor bandwidth. Applying equ.(4) to the hypothetical signal of equ.(1), and assuming a delay $\delta = 100nsec = 0.1T$, we find τ_e decreases with increasing ω_0:

$$\tau_e = \frac{1}{\omega_0} \frac{\alpha R(\tau)}{1 - \frac{R''(0)}{\omega_0^2}} \quad (6)$$

3.4 Tracking Wide Bandwidth Signals

We will briefly describe techniques for tracking wide bandwidth signals, applied to the signal structure of equ.(1). The first approach, described in fig.8 can be implemented in hardware, and is geared towards real-time positioning. The receiver is based on the idea that

[6] This assertion is reasonable, given the conservatism of the analysis. Distortion of the correlation function caused by $m(t)$ will be most severe when the slope, $R'(-\delta)$ is maximal. In this case, $R''(-\delta)$ would be minimal.

each of the codes $C(t)$ can be independently tracked. Precision is provided by the PLL that tracks the *splitting signal* which has frequency ω_0. The DLL tracks the slower codes $C(t)$, and is used to resolve the correct correlation peak from all those present due to the $cos(\omega_0\tau)$ term in $R_y(\tau)$ - see fig. 7. Note in fig.8 that at the output of the code mixers, we show only those terms which will pass through the lowpass filters. Note also, for the sake of clarity, that we have not illustrated early and late correlators which are necessary for an early-minus-late power discriminator in the DLL.

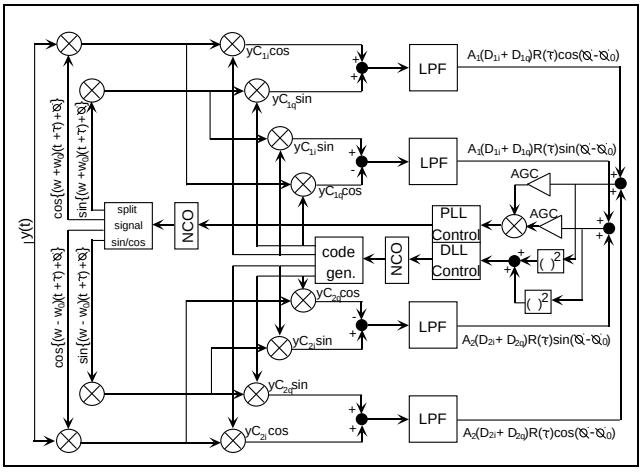

Figure 8: Hardware architecture to track the signal of equ.(1)

The most thorough approach for multipath mitigation is to sample an entire autocorrelation function, rather than to use only early and late samples. In the case that position can be computed with a couple of seconds delay, such as in E911 applications, the best approach is to use a *software receiver*, which samples a sequence of the downconverted signal, and then processes this using a DSP. The following algorithm describes how the complete autocorrelation function can be generated, in a software receiver, based on samples of a signal $y(t)$. Let ω_{in} be the nominal offset of the sampled incident signal, and let ω_{offset} be the largest possible offset frequency, due to Doppler shift and oscillator frequency drift.

* $R_{max} = 0$
* Create a complex wide-bandwidth code signal
  $y_{code}(t) = (C_{i1}(t) + C_{i2}(t))\, cos(\omega_0 t) +$
  $(C_{q1}(t) - C_{q2}(t))\, sin(\omega_0 t) + j\,(C_{q1}(t) + C_{q2}(t))\, cos(\omega_0 t)$
  $+j\,(C_{i2}(t) - C_{i1}(t))\, sin(\omega_0 t), \quad t = [0\ \ldots\ T_i]$
* Compute $F(y_{code})^*$ where F is the fourier-transform operator, and * is the conjugation operator.
* For $\omega = \omega_{in} - \omega_{offset} : \omega_{in} - \omega_{offset}\ step\ \frac{2\pi}{T_i}$
  * Create complex mixing signal
    $y_{mix}(t) = cos(\omega t) + j sin(\omega t), t = [0\ \ldots\ T_i]$
  * Combine the incident and mixing signals
    $y_{comb}(t) = y(t) y_{mix}(t)$
  * Compute $R(\tau) = F^{-1}\,(F(y_{code})^* F(y_{comb}(t)))$
  * If $max_\tau \mid (R(\tau)) \mid > R_{max}$,
    $R_{max} \leftarrow max_\tau \mid R(\tau) \mid, R_{store}(\tau) = R(\tau)$
* Next ω

Upon exit, $R_{store}(\tau)$ will store the correlation between $y(t)$ and the complex code, for however many code periods are represented in the integration time T_i. $R_{store}(\tau)$ may be further refined by searching over smaller steps of ω_o. The initial step size for ω_o must be less then half the Nyquist rate $\frac{2\pi}{T_i}$. Many derivatives of this theme are possible. In addition, the extension to tracking a signal with more than two multiple split signal sidebands is obvious.

3.5 Hypothetical DOP and Navigation Error in Standalone System

At 30dB of attenuation, it is difficult to measure pseudorange from a GPS signal. This is not necessarily the case for a Globalstar signal, which can be integrated for 200msec. We will briefly consider the performance of a system, indoors, for which only the Globalstar signals are available. Multipath error dominates the noise equation. Based on the preceding analysis, and the hypothesis that wideband signals - of bandwidth roughly 10 MHz can be used - the pseudorange error due to multipath is up to 0.5 meters.

Monte-Carlo simulations were conducted to estimate the Geometric Dilution of Precision for the system, as a function of tracking interval. Fig.9 shows HDOP and VDOP separately. The rapid reduction in the DOP is due to the rapid angular velocity of the GSTR satellites. For each tracking interval, a histogram shows the probability distribution of DOPs which results from tracking Globalstar satellites over that interval. Two pseudorange measurements are assumed for each visible satellite: one at the initiation of tracking, and one at the end of the tracking interval. For example, consider the histograms for the 10 second interval. For a wide range of satellite geometries, a pseudo-range measurement is simulated from all visible satellites at time 0 seconds, and then again at time 10 seconds. As such, each satellite generates the same information as two spatially separated satellites [7]. Since only one estimate

[7] We assume that the multipath errors are uncorrelated at the beginning and end of the tracking interval, and as above, we do not account for the fact the satellites may sometimes not be illuminated by a Gateway.

of the receiver clock bias is made, the technique requires a stable quartz oscillator, with Allan Variance better than 10^{-11} over intervals of 10^2 seconds [8]. Based on GDOP, and an estimate of pseudoranging error discussed above, we can estimate the associated position errors. Fig. 10 illustrates the horizontal position error histograms (left) and vertical position error histograms, as a function of tracking interval.

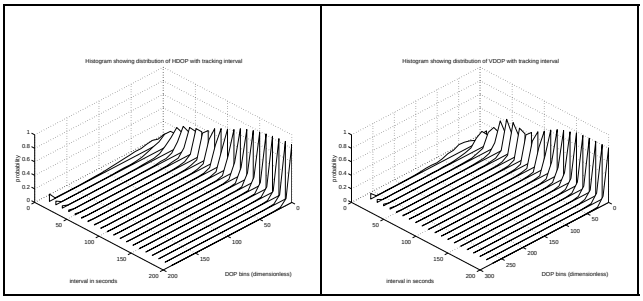

Figure 9: Evolution of Globalstar HDOP and VDOP with Tracking Interval

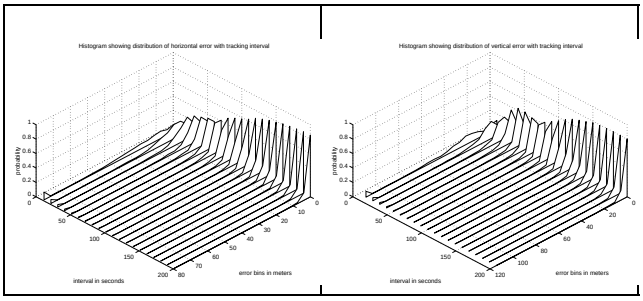

Figure 10: Evolution of Positioning Error with Tracking Interval, using Globalstar as a Standalone Signal

4 LEOS in the Resolution of Integer Cycle Ambiguities for Centimeter-Level Navigation

Before presenting data, we'll describe the algorithm by which integer cycle ambiguities are resolved, and the integrity of the solution bounded. We will not describe in detail the method by which phase measurements are made, and post-processed. Refer to [5, 8] for a discussion of corrections applied to the phase measurements, and to [9, 8] for a description of real-valued parameter estimation techniques. We assume, at the outset of this section, that the user has obtained a real-valued unbiased estimate, $\hat{\mathbf{z}}$, of the integer parameters, $\mathbf{z}$, together with a covariance for those estimates $\mathbf{P}_z$. We can consider the estimate $\hat{\mathbf{z}}$ to be generated by process $\hat{\mathbf{z}} = \mathbf{z} + \mathbf{u}$ where $\mathbf{u}$ is a disturbance distributed as $\sim N(0, \mathbf{P}_z)$. Define the whitening matrix $\mathbf{G} = \mathbf{P}_z^{-\frac{1}{2}}$. The maximum likelihood estimation problem can now be framed as

$$\mathbf{z}_{ML} = \arg \min_{\mathbf{z} \in \mathbf{Z}^{q \times 1}} \|\mathbf{G}\hat{\mathbf{z}} - \mathbf{G}\mathbf{z}\|_2 \tag{7}$$

Given our noise assumptions, we may now compare the relative likelihood of two integers vectors, say $\mathbf{z}_1$ and $\mathbf{z}_2$ according to

$$\frac{Prob(\mathbf{z} = \mathbf{z}_1)}{Prob(\mathbf{z} = \mathbf{z}_2)} = exp(\|\mathbf{G}(\mathbf{z}_2 - \mathbf{z})\|_2^2 - \|\mathbf{G}(\mathbf{z}_1 - \mathbf{z})\|_2^2)$$

However, instead of searching through a large set of integer vectors to find the most likely combination, we would ideally like to establish a lower bound on the confidence with which any particular vector of integers can be selected. This confidence is independent of any particular estimate of the integers. When the confidence is sufficiently high, we would then perform an efficient integer search, considering as few combinations as possible.

As a first step, define the random variable $\bar{\mathbf{z}} = \mathbf{G}\hat{\mathbf{z}}$, $\bar{z} \sim N(\mathbf{G}\mathbf{z}, \mathbf{I}^{q \times q})$. The maximum-likelihood problem of equ. (7) now reads

$$\mathbf{z}_{ML} = \arg \min_{\mathbf{z} \in \mathbf{Z}^{q \times 1}} \|\bar{\mathbf{z}} - \mathbf{G}\mathbf{z}\|_2 \tag{8}$$

The matrix $\mathbf{G}$ is termed the *lattice generator*. It forms the basis of a lattice, $L(\mathbf{G}) = \left\{\mathbf{G}\mathbf{z} \mid \mathbf{z} \in \mathbf{Z}^{q \times 1}\right\}$ which is conceptually illustrated in fig.11 for $q = 2$. For the lattice $L(\mathbf{G})$, each integer point $\mathbf{z}_i$ is associated with a *Voronoi cell* which contains all the points $\bar{\mathbf{z}}$ which are closer to $\mathbf{G}\mathbf{z}_i$ than any other $\mathbf{G}\mathbf{z}_j, j \neq i$. The Voronoi cell for $\mathbf{z}_i$ is $\left\{\bar{\mathbf{z}} \in \mathbf{R}^{q \times 1} \mid \|\bar{\mathbf{z}} - \mathbf{G}\mathbf{z}_i\| < \|\bar{\mathbf{z}} - \mathbf{G}\mathbf{z}_j\|, j \neq i\right\}$

Such a Voronoi cell is illustrated in the fig. 11. The confidence with which a particular integer combination may be selected is found by integrating the probability density function (pdf) of $\bar{\mathbf{z}}$ over the entire volume of a Voronoi cell. However, since the Voronoi cell is defined by multiple hyperplanes, this integral is difficult to compute. In order to make this computation tractable, we approximate a Voronoi cell with the largest ball which can fit therein. All that we require to approximate the the pdf integral is the radius of this ball, which is shown illustrated in fig. 11 as $\frac{d_{min}}{2}$.

[8] This stability could also be obtained from a signal arising from a cellular base station in E911-type applications

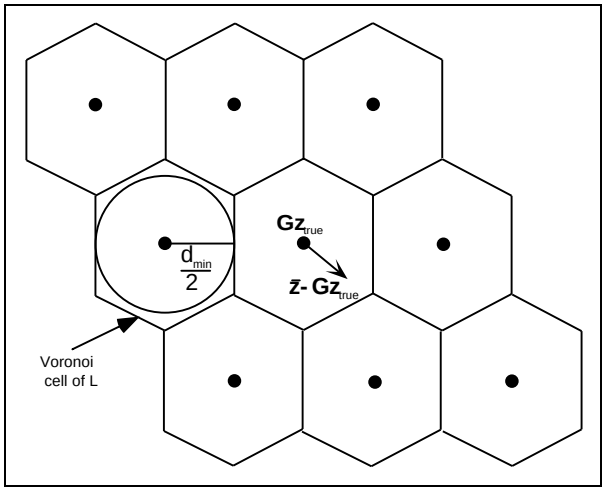

Figure 11: Lattice generated by the generator matrix $\mathbf{G}$

Consider the set of columns which constitute the lattice generator, $\mathbf{G} = [\mathbf{g}_1 \dots \mathbf{g}_q]$. We will describe the Gram-Schmidt orthogonalization of $\mathbf{G}$ as $\mathbf{G}^* = [\mathbf{g}_1^* \dots \mathbf{g}_q^*]$ where

$$\mathbf{g}_j^* = \mathbf{g}_j - \sum_{i=1}^{j-1} \frac{\mathbf{g}_j^T \mathbf{g}_i^*}{\|\mathbf{g}_i^*\|^2} \mathbf{g}_i^*, \ j = 1 \dots q \tag{9}$$

It can be shown [8, 1] that a lower bound on the value of d_{min} can be found according to:

$$d_{min} \geq min(\|\mathbf{g}_1^*\|_2, \|\mathbf{g}_2^*\|_2, \dots \|\mathbf{g}_q^*\|_2) \tag{10}$$

Consider, as an example, the lattice points generated by the 2-D lattice generator

$$\mathbf{g}_1 = \begin{bmatrix} 0.47 \\ 0.62 \end{bmatrix}, \quad \mathbf{g}_2 = \begin{bmatrix} 0.62 \\ 1.10 \end{bmatrix} \tag{11}$$

as shown in fig. 12. Since $\mathbf{g}_1$ and $\mathbf{g}_2$ are almost co-linear, the inequality $d_{min} \geq \|g_2^*\|$ clearly provides a very poor lower bound. This situation is typical for the type of geometries encountered in satellite navigation. In order to compute a tighter lower bound on d_{min} we would like the columns of $\{\mathbf{g}_i\}$ to be as linearly independent as possible. Stated differently, we would like to find a matrix, $\bar{\mathbf{G}}$ which generates exactly the same lattice, but for which the columns $\{\bar{\mathbf{g}}_i\}$ are as orthogonal as possible.

The algorithm of Lenstra-Lenstra-Lovatz [1] provides a computationally efficient technique for deriving a new lattice generator matrix $\bar{\mathbf{G}} = \mathbf{GF}$ where $\mathbf{F}$ is a unitary matrix, and all its elements are integer-valued. As a result, $\bar{\mathbf{G}}$ generates exactly the same lattice points as $\mathbf{G}$. However, the columns of $\bar{\mathbf{G}}$, $\{\bar{\mathbf{g}}_i\}$, are *almost* orthogonal, in the sense that

$$\bar{\mathbf{g}}_j = \sum_{i=1}^{j} \mu_{ji} \bar{\mathbf{g}}_i^*, \ \mu_{jj} = 1, |\mu_{ji}| < \frac{1}{2}, \ \ i \neq j \tag{12}$$

where $\{\bar{\mathbf{g}}_i^*\}$ are the columns of $\bar{\mathbf{G}}^*$, the Gramm-Schmidt orthogonalization of $\bar{\mathbf{G}}$.

By maintaining some degree of linear independence among the columns $\{\bar{\mathbf{g}}_i\}$, the LLL algorithm tightens the bound on d_{min} which is obtained by the Gram-Schmidt technique, $d_{min} \geq min(\|\bar{\mathbf{g}}_1^*\|^2 \dots \|\bar{\mathbf{g}}_q^*\|^2)$. The feature is illustrated in fig. 12. Notice that the vectors $\bar{\mathbf{g}}_1^*$ and $\bar{\mathbf{g}}_2^*$ are *almost* orthogonal, with the result that $min(\|\bar{\mathbf{g}}_1^*\|^2, \|\bar{\mathbf{g}}_2^*\|^2) > min(\|\mathbf{g}_1^*\|^2, \|\mathbf{g}_2^*\|^2)$. As can be seen, a close bound on d_{min} is established by $\|\bar{\mathbf{g}}_2^*\|$.

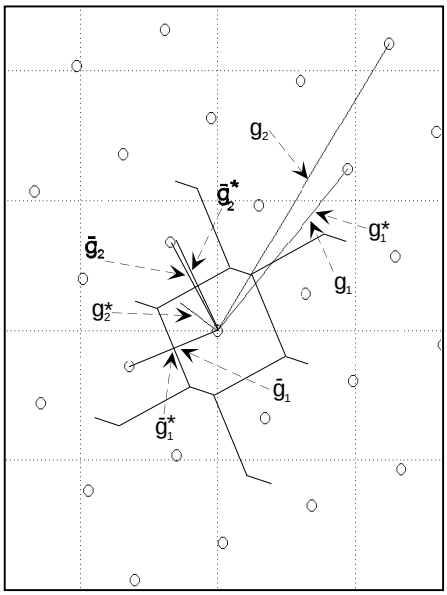

Figure 12: Lattice points, lattice generator vectors, and orthogonal basis vectors

Now, $\|\bar{\mathbf{z}} - \mathbf{Gz}\|^2$ is the sum of q independent normally distributed unit variance random variables. Consequently, this cost has a χ^2 distribution with q degrees of freedom. We denote by $F_{\chi^2}(\chi^2; q)$ the cumulative distribution function of a χ^2 random variable of q d.o.f. Once we have a bound on d_{min}, d, we can find a lower bound on the probability of correct integer selection:

$$Prob\{\mathbf{z}_{ML} = \mathbf{z}\} \geq F_{\chi^2}\left(\frac{d^2}{4}; q\right) \tag{13}$$

This is computed by a lookup into a table describing $F_{\chi^2}(\chi^2; q)$ and is computationally very cheap. Notice that as more measurements are taken over time, and the geometric diversity improves, the magnitude of d_{min} will increase. Consequently, the error involved in integrating the pdf of $\bar{\mathbf{z}}$ over a sphere of radius $\frac{d_{min}}{2}$ rather than over the Voronoi cell $\rightarrow 0$. Hence the lower bound on $Prob\{\mathbf{z}_{ML} = \mathbf{z}\}$ becomes tight.

4.1 An Efficient Integer Search Algorithm

We return now to the integer least-squares estimation problem of equ. (7). Replacing $\mathbf{G}$ by $\bar{\mathbf{G}}$, the estimation problem can be reformulated as

$$\bar{\mathbf{z}}_{ML} = \arg \min_{\mathbf{z} \in \mathbf{Z}^{q \times 1}} (\mathbf{z} - \tilde{\mathbf{z}})^T \mathbf{P}^{-1} (\mathbf{z} - \tilde{\mathbf{z}}) \tag{14}$$

where $\tilde{\mathbf{z}} = \bar{\mathbf{G}}^{-1}\bar{\mathbf{z}}$, $\mathbf{P} = (\bar{\mathbf{G}}^T\bar{\mathbf{G}})^{-1}$. The maximum likelihood integer vector which solves the previous formulation of equ. (7) can be found by the transformation $\mathbf{z}_{ML} = \mathbf{F}\bar{\mathbf{z}}_{ML}$. Notice that if $\mathbf{P}$ is diagonal, then the expression becomes

$$\bar{\mathbf{z}}_{ML} = \arg \min_{\mathbf{z} \in \mathbf{Z}^{q \times 1}} \sum_{i=1}^{q} \frac{(z_i - \tilde{z}_i)^2}{P_{ii}} \tag{15}$$

in which case we can simply find the integers by rounding: $\bar{z}_{ML,i} = \lceil \tilde{z}_i \rfloor$. Since $\bar{\mathbf{G}}$ is *almost* orthogonal, $\mathbf{P}$ is *almost* diagonal, and we can use the rounding of $\tilde{\mathbf{z}}$ as an initial suboptimal estimate of $\bar{\mathbf{z}}_{ML}$, $\bar{\mathbf{z}}_{sub}$. Since we have the lower bound $\frac{d_{min}}{2}$ from equ. (10), we know that if $\|\bar{\mathbf{z}} - \bar{\mathbf{G}}\bar{\mathbf{z}}_{sub}\|_2 < \frac{d_{min}}{2}$ then $\bar{\mathbf{z}}_{sub}$ is the global minimum $\bar{\mathbf{z}}_{ML}$. Consequently, the algorithm we employ for attaining $\mathbf{z}_{ML}$ is as follows:

* Solve real-valued parameter estimation problem [9, 8] to find $\hat{\mathbf{z}}$ and $\mathbf{P}_z$
* Compute $\mathbf{G}$, and $\hat{\mathbf{z}}$ and set $\bar{\mathbf{z}} = \mathbf{G}\hat{\mathbf{z}}$.
* Perform the LLL on the columns of $\mathbf{G}$ to generate a unimodular matrix $\mathbf{F}$ and create a new lattice generator matrix $\bar{\mathbf{G}} = \mathbf{G}F$ which is almost orthogonal.
* $\mathbf{z}_{sub} \leftarrow \mathbf{F}\lceil \bar{\mathbf{G}}^{-1}\bar{\mathbf{z}} \rfloor$. If $\|\bar{\mathbf{z}} - \mathbf{G}\mathbf{z}_{sub}\|_2 < \frac{d_{min}}{2}$ then $\mathbf{z}_{ML} = \mathbf{z}_{sub}$ and stop.
* $r \leftarrow \|\bar{\mathbf{z}} - \mathbf{G}\mathbf{z}_{sub}\|_2$ and $\bar{\mathbf{z}}_{sub} \leftarrow \mathbf{F}^{-1}\mathbf{z}_{sub}$
* while 1
    * Search for an integral point within ellipsoid $\|\bar{\mathbf{z}} - \bar{\mathbf{G}}\mathbf{z}\|_2 < r$. If no such point exists $\mathbf{z}_{ML} \leftarrow \mathbf{F}\bar{\mathbf{z}}_{sub}$ and stop.
    * Let $\bar{\mathbf{z}}_{sub}$ be the integral point found in the previous step. $r \leftarrow \| \bar{\mathbf{z}} - \bar{\mathbf{G}}\bar{\mathbf{z}}_{sub} \|_2$.
    * If $r \leq \frac{d_{min}}{2}$ then $\mathbf{z}_{ML} \leftarrow \mathbf{F}\bar{\mathbf{z}}_{sub}$ and stop.
* end.

Note that when we search within the ellipsoid $\|\bar{\mathbf{z}} - \bar{\mathbf{G}}\mathbf{z}\|_2 < r$ we seek an integral point as close to the center of the ellipsoid as possible. An efficient approach to performing this search is discussed in [1, 8]. Once the integer parameters are identified using any of the techniques discussed above, they can be regarded as constant biases. The receiver uses these biases to update position estimates with centimeter-level precision in real time [8].

5 Experimental Results

In this section, we present results from tracking Orbcomm in conjunction with GPS. Fig's 13, 14, 15 display data for 4 separate overpasses of single Orbcomm satellites. These passes have been labelled $a-d$. Notice that each of the LEO passes were almost directly overhead. This type of pass is, of course, atypical. For rapid acquisition of precise position, one would ideally track multiple LEO satellites in conjunction with GPS. Nonetheless, this data illustrates the performance enhancement that can be achieved using just a single LEO. An intuitive explanation of this effect is provided in [9]. Fig. 13 illustrates the evolution of the lower bound on the probability of selecting the correct set of integer parameters for all satellites being tracked. This lower bound is computed by the technique discussed above, and becomes tight as the probability $\rightarrow 1$. Fig. 14 illustrates the actual maximum-likelihood integer estimates, computed over the course of tracking. Notice that in all cases, cycle ambiguities are resolved in well under one minute. Finally, fig. 15 illustrates the resulting position errors after cycle ambiguities are resolved. These errors fit roughly within a the volume of a golf-ball. The user and reference receivers are close enough that thermal noise rather than ionospheric/tropospheric effects determine the noise floor.

6 Conclusions

LEO satellites provide a powerful complement to GPS, both for meter-level navigation in disadvantaged environments, and for precision navigation outdoors. LEOs provide additional ranging signals, which improve GDOP, availability of navigation solutions, and

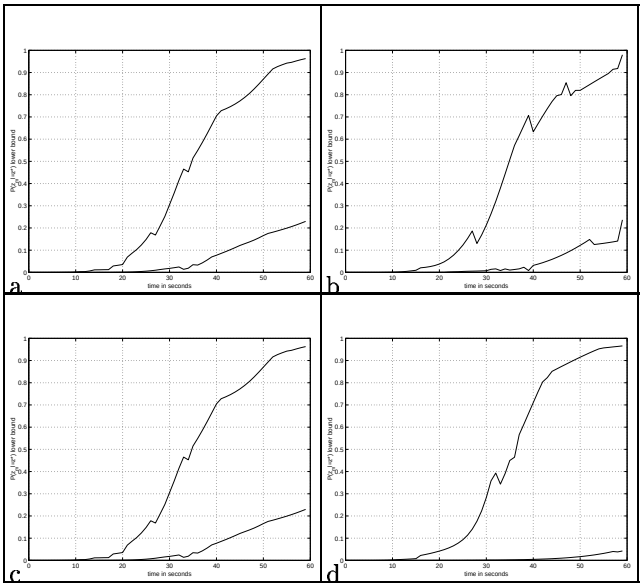

Figure 13: Evolution in the lower bound on the probability of selecting the correct set of integer cycle ambiguities over 60 seconds of tracking. Probability is plotted using the GPS signals alone, as well as for the GPS signals combined with a single Orbcomm satellite signal. The performance enhancement is considerable.

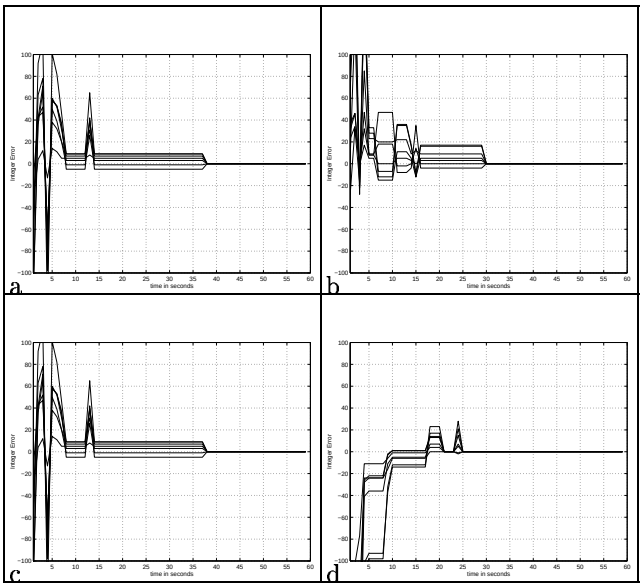

Figure 14: Maximum-likelihood integers estimates over 60 seconds of tracking GPS satellites together with a single Orbcomm satellite. Notice that in all cases, the cycle ambiguities are resolved well within one minute.

availability of RAIM geometry. The signals transmitted by certain LEOs are of sufficient bandwidth to substantially enhance their multipath performance. The rapid angular motion of the satellites provides the geometric diversity required for resolution of cycle ambiguities for centimeter-level navigation outdoors, as well as for stand-alone positioning (without GPS) in highly attenuating environments. LEO signals, such as the pilot signals of Globalstar, can be integrated for a longer time than those of GPS. We have demonstrated the resolution of cycle ambiguities by tracking Orbcomm in conjunction with GPS. The data reduction techniques which we describe eliminate the need for expensive dual-frequency GPS receivers with precalibrated radio frequency circuitry. In fact,the front end for a Globalstar receiver, which is capable of achieving centimeter-level performance, is shown next to a cell-phone in fig. 16. All the components for this front end cost under 10 Dollars combined.

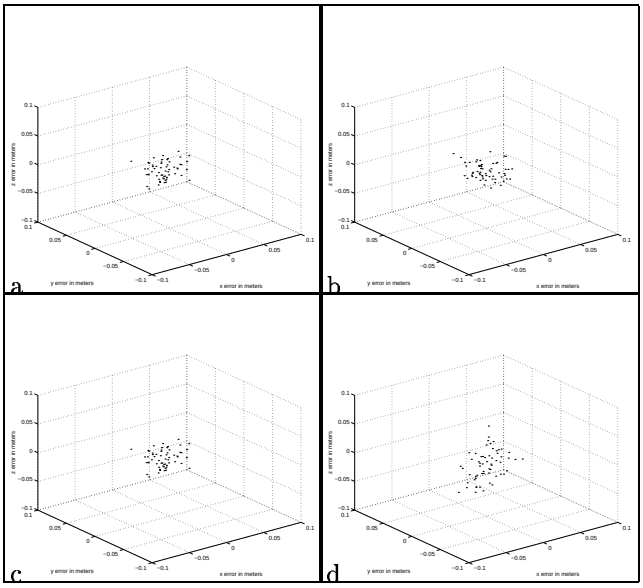

Figure 15: Position errors after resolving the cycle ambiguities on GPS and a parameter related to the cycle ambiguity on an Orbcomm satellite. Notice that position errors fit roughly within the size of a golf-ball.

References

[1] A.Hassibi. Integer paramter estimation in linear models with application to GPS. Technical Report ECS-9222391, Information Systems Laboratory, Stanford University, 1996.

[2] P.Fenton A.J van Dierendonck, M.Schumpert. Acquisition, tracking and mitigating multipath using the proposed split spectrum c/a-code at l2. *Proceedings of ION-GPS 98*, pages 1895–1903, 1998.

[3] T.Ford A.J van Dierendonck, P.Fenton. Theory and performance of narrow correlator spacing in a GPS receiver. *Navigation*, 39(3):265–283, 1992.

Figure 16: Front end for a Globalstar Navigation Receiver

[4] C.C. Hodge D.W. Allan, N. Ashby. The science of timekeeping. Technical Report Application Note 1289, Hewlett Packard, 1997.

[5] M.Rabinowitz et al. A system using leo telecommunication satellites for rapid acquisition of integer cycle ambiguities. *IEEE PLANS 98*, April 1998.

[6] A.J. Van Dierendonck J.J. Spilker Jr. Proposed new civil gps signal at 1176.45 mhz. *Proceedings of ION GPS99*, pages 1717–1725, 1999.

[7] B.W. Parkinson J.J. Spilker Jr., E.H. Martin. A family of split spectrum gps civil signals. *Proceedings of ION GPS98*, pages 1905–1914, 1998.

[8] M.Rabinowitz. *PhD Thesis: Precision Navigation Using Low Earth Orbit Telecommunication Satellites.* PhD thesis, Department of Electrical Engineering, Stanford University, 2000.

[9] B.W.Parkinson M.Rabinowitz, K.Gromov and C.E.Cohen. Architectures for joint gps/leo satellite carrier phase receivers designed for rapid robust resolution of carrier cycle ambiguities on mobile platforms. *Proceedings of the Institute of Navigation ION GPS-2000*, September 2000.

[10] C.E.Cohen M.Rabinowitz and B.W.Parkinson. The application of leos to cycle anbiguity resolution on navstar transmissions for kinematic carrier-phase positioning. *Institute of Navigation, ION97*, 1(1), September 1997.

[11] C.E.Cohen M.Rabinowitz and B.W.Parkinson. Patent application: Resolving integer cycle ambiguities with LEO satellites. Technical Report 60/041,184, Application: US Patent and Trademark Office, March 1998.

[12] M.Moeglein N.Krasner. An introduction to snaptrack server-aided gps technology. *Proceedings Of IONGPS98*, pages 333–342, 1999.

[13] A.V. Oppenheim and R.W.Schafer. *Discrete-Time Signal Processing.* Prentice-Hall, Inc., 1989.

[14] B.W. Parkinson and P. Axelrad. Autonomous integrity monitoring using the pseudorange residual. *Navigation: Journal of the Institute of Navigation*, 35(2), 1988.

[15] A.J van Dierendonck. GPS receivers. *Global Positioning System: Theory and Applications*, 1:329–408, 1995.

[16] G.W. Torrence W.J. Vogel. Propagation measurements for satellite radio reception inside buildings. *IEEE Transactions on Antennas and Propagation*, 41(7):954–961, July 1993.

[17] H.P. Lin W.J. Vogel, G.W. Torrence. Slant-path building penetration measurements at l- and s-band. Technical Report EERL Technical Report EERL-95-301, The University of Texas, Electrical Engineering Research Laboratory, 1995.

[18] J. Goldhirsh W.J. Vogel. Propagation effects for land mobile satellite systems: Overview of experimental and modeling results. Technical Report Reference Publication 1274, NASA, 1992.

[19] H.P.Lin W.J.Vogel, G.W.Torrence. Into building fading at l- and s-band for satellite pcs. *Proceedings of the Nineteenth NASA Propagation Experimenters Meeting (NAPEX XIX) and the Seventh Advanced Communications Technology Satellite (ACTS) Propagation Studies Workshop (APSW VII), (JPL Publication 95-15), Fort Collins, Colorado*, June 1995.